Adsorption Isotherms of Pure Gas and Binary Mixtures of Air Compounds on Faujasite Zeolite Adsorbents: Effect of Compensation Cation

Marie L. Zanota,[†] Nicolas Heymans,[†] Frédéric Gilles,[‡] Bao L. Su,[‡] Marc Frère,[†] and Guy De Weireld*[,†]

University of Mons, Faculté Polytechnique, Thermodynamics Department, 31 Bd Dolez 7000 Mons, Belgium, and University of Namur, Laboratory of Inorganic Materials Chemistry, 61 Rue de Bruxelles 5000 Namur, Belgium

To design or simulate air separation by a pressure swing adsorption process (PSA), adsorption equilibrium data in the range of temperatures used in this kind of process are needed. Acquisition of coadsorption equilibrium data is time-consuming, and then a binary model based on pure substance isotherm measurements is usually used to simulate equilibrium in PSA. In this paper, adsorption equilibrium data for nitrogen and oxygen on five faujasite zeolites (NaX, NaLSX, KLSX, and two LiLSX) were obtained at (288, 303, and 318) K and at pressures up to 3000 kPa. Coadsorption equilibria of nitrogen and oxygen mixtures were measured at 400 kPa with an original volumetric apparatus which is able to keep a constant pressure in the measurement cell. The measurements were compared to isotherms calculated by an extended Langmuir−Freundlich model. The influence of compensation cation on the adsorption capacities and selectivities was also analyzed.

Introduction

Production of pure oxygen or air enriched in oxygen[1,2] is an important stage in industrial processes such as wastewater treatment or oxycombustion. In wastewater treatment, air enriched in oxygen allows a decrease in the energetic costs of gas pressurization by pressurizing oxygen with less nitrogen. In oxycombustion techniques, the outlet streams have a higher carbon dioxide concentration; considering the carbon dioxide concentration level, a capture unit of carbon dioxide is not necessary, and dry smokes can be directly compressed and stored. A low nitrogen concentration leads to a better efficiency of the process, and it also allows a cost reduction and a better treatment of industrial flue contaminant gases. This last point is essential for limiting environmental impact and the fulfillment of international regulations. It is important that the process, designed for oxygen or enriched air production, uses as little energy as possible to ensure low production costs.

Air separation techniques using a pressure swing were disclosed in 1950.[3] Pressure swing adsorption (PSA) processes with two beds and four operation steps, which are (1) pressurization with feed, (2) high pressure feed with product withdrawal, (3) depressurization, and (4) desorption at low pressure with purge, are commonly attributed to Skarstrom.[4] Separation processes such as PSA, vacuum swing adsorption (VSA), and vacuum pressure swing adsorption (VPSA) are known to be characterized by a low-energy consumption compared to other techniques such as cryogenic distillation.[5,6] Their reliability and ability to produce high-purity compounds make them more suitable than membrane techniques.[7−9] PSA, VSA, and VPSA have been largely described in the literature.[10,11] The specific energy consumption of early PSA plants, operating completely above atmospheric pressure, was as high as 1 kWh/Nm^3. Modern plants with vacuum regeneration (VSA) need less than 0.4 kWh/Nm^3 to produce a 93 % oxygen mixture. At the same time, investment costs could be significantly reduced by increasing adsorption capacity and selectivity of the plants. This was achieved by the improvement of zeolite adsorbents as well as optimization of the process. They are the object of many developments on the scientific side (high selectivity adsorbent, process, and simulation tools)[12−24] as well as on the technological side (rotative adsorbent, compacted design, or three bed design with two different adsorbents).[25−27]

As far as air separation is concerned, it is well-known that X type faujasites have good separation performances.[28] These performances can be improved if the Si/Al ratio tends toward one and/or if the compensation cation is exchanged with the Li cation.[23,29,30] It is quite difficult to obtain on the one hand a very low Si/Al ratio (close to 1) and, on the other hand, a high Li cation fraction content. Li cation zeolites cannot be synthetized directly, and a Li ion exchange technique is expensive and time-consuming. Consequently, the ideal adsorbent may appear to be costly. Furthermore, it is not always necessary to produce oxygen at high purity since there are many industrial applications which just need oxygen-enriched air.[31] Therefore, it is interesting to evaluate and compare separation performances for different zeolites like NaX or NaLSX zeolites because their use may be justified for economic reasons in processes where high oxygen purity is not required.

This paper is devoted to the study of nitrogen/oxygen separation capacities of five types of faujasite zeolites. Those capacities depend on zeolite selectivity. Coadsorption nitrogen/oxygen equilibrium isotherms are then needed. Measuring coadsorption equilibrium data is time-consuming and tedious compared to pure gas data. The simulation of mixture equilibrium from pure gas isotherms is then an easier way to compare adsorbent to one another.

Here, we present experimental adsorption equilibrium data of pure nitrogen and oxygen. These data consist of adsorption isotherms at three temperatures, (288, 303, and 318) K, carried out using a volumetric apparatus for pressures from 10 kPa up to 3000 kPa on a tailor-made volumetric apparatus. The experimental procedure has been developed in such a way that the accuracy of the measurements can be determined.[32] Pure

* Corresponding author. E-mail: guy.deweireld@umons.ac.be.
[†] University of Mons.
[‡] University of Namur.

10.1021/je900539m
Published on Web 12/17/2009

Table 1. Chemical Compositions and Characteristics of the Studied Zeolites

zeolite	chemical composition	Si/Al ratio	pore size diameter Å	pore volume $cm^3 \cdot g^{-1}$	specific surface area $m^2 \cdot g^{-1}$
NaX	$Na_{86}Al_{86}Si_{106}O_{384}$	1.20	5.1	0.232	527
NaLSX	$Na_{96}Al_{96}Si_{96}O_{384}$	1.00	5.0	0.250	629
KLSX	$K_{96}Al_{96}Si_{96}O_{384}$	1.00	5.1	0.201	501
LiLSX	$Li_{94.4}Na_{0.2}K_{1.4}Al_{96}Si_{96}O_{384}$	1.00	5.0	0.269	688
$LiLSX^{hm}$	$Li_{93.8}Na_{1.7}Al_{95.5}Si_{96.5}O_{384}$	1.01	5.2	0.254	636

gas isotherms were used to evaluate the parameters of a Langmuir−Freundlich theoretical model usually used in PSA process simulations.[27,34] Coadsorption nitrogen/oxygen equilibria have been measured at 400 kPa and 303 K on an original volumetric apparatus[33] and have been compared with equilibrium data obtained with the Langmuir−Freundlich model.

Experimental Section

Material Synthesis and Characterization. NaX (Si/Al = 1.2) was provided by Süd-Chemie AG. NaLSX, KLSX, and LiLSX (Si/Al = 1.0) were provided by Tricat Zeolites GmbH. Another homemade LiLSX was also studied. This one is noted $LiLSX^{hm}$. It was obtained by ion exchange of a NaKLSX in a concentrated solution of LiCl. The NaKLSX was synthesized from sodium aluminosilicate gel having the oxide molar ratio $SiO_2/Al_2O_3 = 2.2$, $(Na_2O + K_2O)/SiO_2 = 3.25$, $Na_2O/(Na_2O + K_2O) = 0.77$, $H_2O/(Na_2O + K_2O) = 17.17$, and $NH_3/Al_2O_3 = 0.26$, by hydrothermal aging at 343 K for 24 h. The solid product was recovered by filtration and washed several times with distilled water to remove excess alkali. The product was then dried at 393 K for one night. N_2 adsorption−desorption isotherms were measured at 77 K on a Micromeritics ASAP 2010 instrument. The samples were first degassed under vacuum at 593 K for several hours. The surface areas were determined using the BET equation in the low pressure region (p/p_0 between 0.05 and 0.25). The nitrogen adsorption−desorption isotherms, obtained on these materials, are typical of microporous materials with specific surface areas varying from 501 $m^2 \cdot g^{-1}$ for the KLSX zeolite up to 688 $m^2 \cdot g^{-1}$ for the LiLSX zeolite. The microporous volumes are determined by the Dubinin equation. Those values are contained between 0.201 $cm^3 \cdot g^{-1}$ for the KLSX zeolite and 0.269 $cm^3 \cdot g^{-1}$ for the LiLSX one. Specific surface areas, microporous volumes, chemical compositions, determined by atomic absorption, and other characteristics of the studied samples are reported in Table 1.

Measurement Procedure. Pure Gas Adsorption. A volumetric apparatus especially developed for pure gas adsorption isotherm acquisition is used in this study.[32] This apparatus (Figure 1), located in an air-refrigerated room (Rr), can provide automated adsorption isotherm measurements for pressures from vacuum up to 3000 kPa and for temperatures ranging from (278 to 333) K.

It is composed of: the pressure cell (PrC); the adsorption cell (AdsC); the control unit (CU); the refrigerated room (Rr); the pressure transmitter (PT) (BARATRON 627B (45 °C) type) provided by MKS; a network of stainless steel tubes; two manual valves (V1 and V2); two electrovalves (EV1 and EV2); two Pt 100 temperature probes (TT1 and TT2); a filter (F); a vacuum pump (VP) to realize a vacuum level lower than 10^{-5} kPa; an in situ heating system (HS) located in the adsorption cell.

The volumetric method is simple in its principle but requires a careful realization of each step of the experimental procedure to obtain reliable data. The uncertainties on the gas volume calibration and on the pressure measurements are the main sources of errors, which may lead to nonrealistic adsorption data.[35−39]

The zeolite is first introduced in the adsorption cell. To eliminate the totality of adsorbed water and gases on the surface of the adsorbent, it is outgassed in situ, the pretreatment procedure depending on the adsorbent. For zeolites, a vacuum is made in the adsorption cell for one hour at ambient temperature. The adsorption cell is then heated up to 673 K with a rate of 1 K per minute. The final temperature and vacuum conditions are kept constant for eight hours.

This procedure is used before all adsorption experiments. The mass of each new sample is measured after the degassing procedure by weighing it on a precision balance, and the volume of the adsorption cell V_{AdsC} is measured by expansion of helium, considered as a nonadsorbed gas.

During isotherm acquisition, a defined amount of gas is first introduced in the pressure cell (PrC) by means of electrovalve EV1. When thermal and mechanical equilibria are reached, the initial pressure p_i and temperature T are recorded. Those measurements (p_i, T, V_{PrC}) provide the initial mole number of gas n_1. The Helmholtz equation of state was used for calculating the gas density (nitrogen,[40] oxygen[41]). Second, the electrovalve EV2 is opened, and the gas expands in the whole installation (pressure cell + adsorption cell) while adsorption occurs. After equilibrium is reached, the pressure and temperature are recorded, and the mole number n_2 of adsorbate remaining in the gas phase is calculated with the new conditions (p_f, T, $V_{PrC} + V_{AdsC}$). The adsorbed mole number n is calculated by the difference ($n_1 - n_2$). The whole isotherm is recorded by successive steps of gas admission and adsorption.

The complete description of the experimental device and procedure can be found elsewhere.[32,36,42,43]

Binary Gas Adsorption. The coadsorption volumetric apparatus specially developed for isobar and isotherm experiments is presented in Figure 2.

It is also composed of an adsorption cell (AdsC); a thermostated room (Rr); a pressure transmitter (PT) (Cerabar PMP 731 provided by Endress Hauser); two manual valves (V1, V2); Pt 100 temperature probes (T); a filter (F); a vacuum pump (VP) to realize a vacuum level lower than 10^{-5} kPa; an in situ heating

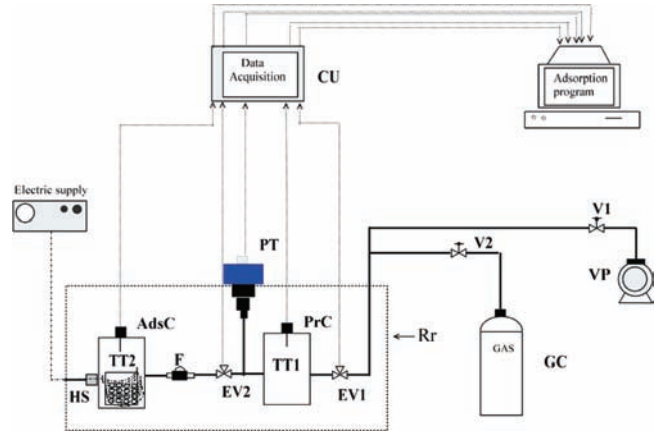

Figure 1. Schematic diagram of the adsorption apparatus.

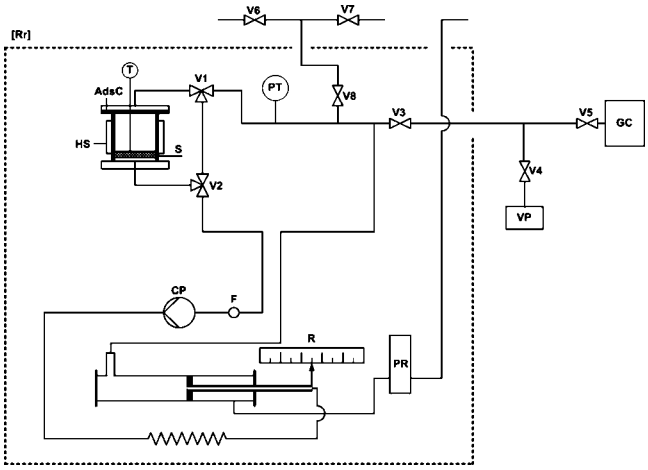

Figure 2. Schematic diagram of coadsorption volumetric apparatus.

system (HS) located in the adsorption cell. A circulation pump (CP) allows a homogeneous mixture to be obtained. A piston is used to modify the total volume of the cells so the pressure is kept at a predefined constant value during adsorption. The position of the piston enables the total volume of the installation to be known exactly. A gas chromatograph (GC) is used to determine the mixture composition before and after adsorption.

The adsorbent is placed in the adsorption cell and is outgassed following a procedure similar to the one used for pure gas adsorption.

The two gases are introduced into the apparatus, and the gas composition is controlled by chromatographic analysis (every 20 min). When the mixture is homogeneous, two successive chromatographic analyses are performed, and the pressure, temperature, and piston position are recorded, allowing the calculation of the mole number of each gas present in the system by using a Kunz and Wargner model.[37] The adsorption cell is then opened (by opening valves V1 and V2), and the piston is moved to obtain the new desired pressure. After the equilibrium is reached, the temperature, pressure, and piston position are recorded once again. Then the adsorption cell is isolated (by closing valves V1 and V2) before the chromatographic analyses are performed. In this way, we avoid any desorption due to a pressure decrease during the analyses.

Before starting the measurements, some tests are performed to estimate the time required to reach equilibrium. Therefore, for each new adsorbent experiment, mixture composition variation is measured over a long period of time. For the five zeolites studied here, the time required before reaching equilibrium is about four hours. The composition analyses are then performed six hours after adsorption has started. The adsorbed amount of each gas is calculated in a similar way to the simple gas isotherm by taking the difference between the number of moles of gases present after adsorption and the number of moles of gases introduced.

Measurement Uncertainties. Pure Gas Isotherm. The pressure is measured using an MKS-BARATRON pressure transmitter with a manufacturer uncertainty of 0.16 % of full scale. For temperature measurements, the Pt 100 probes are characterized by an uncertainty equal to 0.15 K. Volumes are determined by helium expansion using a calibrated reference cell volume. The estimated uncertainties on volumes are equal to 2 %. The maximum deviation between calculated and experimental densities is reported to be lower than 0.02 % for nitrogen[40] and lower than 0.25 % for oxygen[41] for the temperatures and pressures used.

The measurement errors on the adsorbed quantities can be calculated from the errors on $P-T-V$ measurements taking into account the calculation procedure. The effects on the adsorbed quantities can be computed for each kind of error separately (pressure, temperature, volumes, gas densities obtained from the equation of state). Such an analysis can be found elsewhere.[32]

For pure gas isotherm measurements, uncertainties increase with pressure because the adsorbed quantities at each pressure are calculated using the adsorbed quantities at the previous pressure. For this study, the computed relative uncertainty on the adsorbed amount varies from 0.5 % for the first recorded point (low pressure) to 2.4 % for the last point for nitrogen and 7 % for oxygen on LiLSX^{hm} at 303 K.

Coadsorption Measurement. For binary systems, it is necessary to take into account the measurement uncertainty due to chromatographic analysis. For this purpose, for each composition determination, we have performed five analyses to estimate the variation in the mixture composition and the related uncertainty. The pressure transmitter has an announced uncertainty of 0.1 % of full scale. For temperature and volume measurements, associated uncertainties are the same as for pure gas measurements. For each equilibrium measurement, we have calculated the uncertainty associated to the adsorbed quantities and to the mixture mole fraction.

Theory. The Langmuir−Freundlich isotherm equation (eq 1) is widely used for fitting isotherm data of nitrogen and oxygen in PSA processes.[38,39,44]

$$Q_{ads} = q_S \frac{bp^{\alpha}}{1 + bp^{\alpha}} \tag{1}$$

in which Q_{ads} is the adsorbed mole number per unit of mass of adsorbent (mmol·g^{-1}); p is the pressure (kPa); q_S is the adsorbed mole number per unit of mass of adsorbent (mmol·g^{-1}) at adsorbent saturation; b is the energetic Langmuir parameter (kPa$^{-\alpha}$); and α is the Langmuir−Freundlich exponent. The three last parameters are the Langmuir−Freundlich parameters.

It can be extended for binary-component adsorption systems (eqs 2 and 3).

$$Q_{ads,A} = q_{S,A} \frac{b_A(py_A)^{\alpha_A}}{1 + b_A(py_A)^{\alpha_A} + b_B(py_B)^{\alpha_B}} \tag{2}$$

$$Q_{ads,B} = q_{S,B} \frac{b_B(py_B)^{\alpha_B}}{1 + b_A(py_A)^{\alpha_A} + b_B(py_B)^{\alpha_B}} \tag{3}$$

$Q_{ads,A}$ and $Q_{ads,B}$ are the adsorbed mole number of A or B per unit of mass of adsorbent (mmol·g^{-1}); $q_{S,A}$, $q_{S,B}$, b_A, b_B, α_A, and α_B are Langmuir−Freundlich parameters for compound A or B; and y_A and y_B are the mole fraction of A or B in the gas phase.

Experimental Results. The gases used for this study (nitrogen, oxygen, and helium) were provided by Praxair Belgium and have a claimed purity equal to 99.999 % vol.

To assess the accuracy of the volumetric measurements, they have been compared to similar ones obtained by a gravimetric apparatus. For the LiLSX^{hm} zeolite at 318 K, the average discrepancy between the two sets of data is lower than 3 % over the whole measurement range.

Data for pure gas isotherms on the five zeolites at 288 K, 303 K, and 318 K are reported in Tables 2 to 6 for nitrogen and in Tables 7 to 11 for oxygen. Excess isotherms are presented in Figures 3 to 7. Coadsorption equilibria at 303 K and 400 kPa are presented in Figures 8 to 12 and in Tables 12 to 16.

Table 2. N_2 Excess Adsorbed Amount on NaX Zeolite As a Function of Pressure at (288, 303, and 318) K

T/K = 288		T/K = 303		T/K = 318	
p/kPa	Q_{ads}/mmol·g^{-1}	p/kPa	Q_{ads}/mmol·g^{-1}	p/kPa	Q_{ads}/mmol·g^{-1}
10	0.066	14	0.061	13	0.042
29	0.186	36	0.156	38	0.121
51	0.311	61	0.258	61	0.189
72	0.426	82	0.346	85	0.260
98	0.558	106	0.436	110	0.328
122	0.673	133	0.531	138	0.405
150	0.794	161	0.626	165	0.474
181	0.921	193	0.727	194	0.546
212	1.039	224	0.822	227	0.623
247	1.162	256	0.914	266	0.709
285	1.289	294	1.013	306	0.794
331	1.425	333	1.113	345	0.874
381	1.566	387	1.237	402	0.981
454	1.740	462	1.390	463	1.088
554	1.951	568	1.584	561	1.243
656	2.143	677	1.763	673	1.404
762	2.319	784	1.920	780	1.547
874	2.481	896	2.066	896	1.685
988	2.626	1026	2.214	1006	1.803
1110	2.765	1152	2.343	1121	1.916
1236	2.890	1275	2.457	1243	2.024
1359	3.001	1408	2.565	1374	2.130
1501	3.111	1544	2.666	1511	2.230
1644	3.212	1696	2.763	1646	2.321
1794	3.305	1845	2.850	1794	2.408
1956	3.396	2002	2.933	1944	2.491
2126	3.479	2168	3.012	2127	2.579
2315	3.558	2351	3.088	2323	2.664
2538	3.641	2573	3.165	2540	2.748
2846	3.734	2866	3.254	2842	2.845

Table 3. N_2 Excess Adsorbed Amount on NaLSX Zeolite As a Function of Pressure at (288, 303, and 318) K

T/K = 288		T/K = 303		T/K = 318	
p/kPa	Q_{ads}/mmol·g^{-1}	p/kPa	Q_{ads}/mmol·g^{-1}	p/kPa	Q_{ads}/mmol·g^{-1}
13	0.069	14	0.051	12	0.036
34	0.179	35	0.131	35	0.098
66	0.337	59	0.215	58	0.161
88	0.441	92	0.329	82	0.222
112	0.545	120	0.420	108	0.288
137	0.650	147	0.504	135	0.352
164	0.759	174	0.587	163	0.420
193	0.866	209	0.686	196	0.493
224	0.972	241	0.773	229	0.565
257	1.082	273	0.857	264	0.640
293	1.195	312	0.952	302	0.717
336	1.317	357	1.057	341	0.793
385	1.448	399	1.150	396	0.892
459	1.619	465	1.279	460	1.002
557	1.822	575	1.472	562	1.157
663	2.018	677	1.636	664	1.302
768	2.191	795	1.798	773	1.441
879	2.346	901	1.933	889	1.573
993	2.486	1027	2.068	1002	1.692
1112	2.612	1143	2.184	1118	1.802
1236	2.726	1266	2.291	1242	1.906
1363	2.829	1391	2.392	1369	2.006
1498	2.925	1528	2.490	1501	2.098
1644	3.017	1662	2.573	1641	2.188
1803	3.105	1807	2.655	1792	2.277
1959	3.181	1964	2.736	1952	2.361
2128	3.254	2167	2.823	2126	2.444
2316	3.325	2353	2.900	2320	2.527
2545	3.397	2563	2.972	2548	2.612
2849	3.478	2850	3.055	2853	2.709

Results and Comments

All pure gas excess isotherms at (288, 303, and 318) K are presented in Figures 3 to 7. As seen from these figures, for all zeolites, the slope of the nitrogen isotherms increases very quickly at low pressure, and the adsorbed amount reaches a constant value at high pressure while the oxygen isotherms are more or less linear. Independent of the adsorbate and temper-

Table 4. N_2 Excess Adsorbed Amount on KLSX Zeolite As a Function of Pressure at (288, 303, and 318) K

T/K = 288		T/K = 303		T/K = 318	
p/kPa	Q_{ads}/mmol·g^{-1}	p/kPa	Q_{ads}/mmol·g^{-1}	p/kPa	Q_{ads}/mmol·g^{-1}
11	0.033	13	0.026	14	0.024
37	0.113	39	0.084	39	0.066
60	0.180	62	0.135	64	0.108
84	0.249	90	0.194	93	0.154
112	0.327	117	0.247	124	0.201
141	0.402	143	0.298	153	0.245
176	0.487	170	0.350	182	0.286
214	0.577	200	0.405	221	0.340
245	0.647	232	0.460	267	0.400
289	0.738	274	0.531	296	0.439
324	0.809	313	0.593	340	0.495
375	0.901	352	0.653	384	0.546
421	0.983	403	0.727	441	0.611
479	1.077	466	0.812	485	0.659
580	1.219	566	0.935	589	0.761
689	1.355	675	1.055	694	0.857
797	1.477	793	1.172	798	0.945
911	1.590	903	1.274	907	1.031
1029	1.694	1013	1.364	1017	1.110
1147	1.786	1137	1.457	1135	1.187
1272	1.873	1261	1.538	1255	1.260
1397	1.950	1379	1.610	1389	1.334
1536	2.026	1602	1.718	1531	1.405
1671	2.093	1783	1.805	1676	1.471
1818	2.157	1914	1.864	1819	1.532
1975	2.220	2054	1.917	1982	1.593
2143	2.278	2210	1.970	2159	1.654
2330	2.335	2390	2.024	2355	1.713
2554	2.394	2588	2.079	2563	1.772
2854	2.458	2854	2.140	2850	1.839

Table 5. N_2 Excess Adsorbed Amount on LiLSX Zeolite As a Function of Pressure at (288, 303, and 318) K

T/K = 288		T/K = 303		T/K = 318	
p/kPa	Q_{ads}/mmol·g^{-1}	p/kPa	Q_{ads}/mmol·g^{-1}	p/kPa	Q_{ads}/mmol·g^{-1}
12	0.211	9	0.109	8	0.058
25	0.390	26	0.267	25	0.169
40	0.548	42	0.396	44	0.284
58	0.710	60	0.529	66	0.395
79	0.870	81	0.660	87	0.496
102	1.021	106	0.794	111	0.600
128	1.162	131	0.917	138	0.707
159	1.299	158	1.030	168	0.817
192	1.433	192	1.152	197	0.914
225	1.555	227	1.270	233	1.022
271	1.687	266	1.391	275	1.132
322	1.823	312	1.508	323	1.245
388	1.961	367	1.634	379	1.368
464	2.102	447	1.786	456	1.502
573	2.254	548	1.942	556	1.654
678	2.402	665	2.094	667	1.801
798	2.536	774	2.232	782	1.936
907	2.657	885	2.349	892	2.057
1015	2.763	999	2.468	1020	2.173
1136	2.872	1133	2.581	1136	2.283
1264	2.974	1256	2.688	1270	2.386
1401	3.077	1381	2.780	1394	2.482
1540	3.173	1523	2.881	1519	2.571
1690	3.271	1656	2.975	1654	2.662
1838	3.362	1809	3.062	1808	2.754
1998	3.444	1970	3.160	1961	2.839
2162	3.537	2136	3.240	2133	2.925
2343	3.613	2339	3.331	2323	3.021
2561	3.708	2563	3.422	2553	3.110
2849	3.794	2849	3.515	2844	3.209

Table 6. N_2 Excess Adsorbed Amount on Homemade LiLSX^{hm} Zeolite As a Function of Pressure at (288, 303, and 318) K

T/K = 288		T/K = 303		T/K = 318	
p	Q_{ads}	p	Q_{ads}	p	Q_{ads}
kPa	mmol·g^{-1}	kPa	mmol·g^{-1}	kPa	mmol·g^{-1}
7	0.155	10	0.138	10	0.086
21	0.388	28	0.319	28	0.224
38	0.606	47	0.494	48	0.355
58	0.799	70	0.652	70	0.469
80	0.985	94	0.794	93	0.584
104	1.138	120	0.928	117	0.691
130	1.273	149	1.054	148	0.817
162	1.418	187	1.189	183	0.925
196	1.547	218	1.291	216	1.034
232	1.668	251	1.393	254	1.135
274	1.789	291	1.495	298	1.237
323	1.911	333	1.590	345	1.340
381	2.034	386	1.693	393	1.434
455	2.167	458	1.825	474	1.564
556	2.318	559	1.966	579	1.705
663	2.453	668	2.109	683	1.837
772	2.579	777	2.234	796	1.952
885	2.687	902	2.350	902	2.059
1002	2.788	1014	2.440	1018	2.157
1127	2.889	1129	2.531	1134	2.247
1256	2.972	1254	2.622	1259	2.328
1383	3.055	1392	2.704	1395	2.409
1517	3.130	1530	2.778	1530	2.482
1667	3.205	1669	2.852	1665	2.555
1810	3.271	1813	2.926	1807	2.619
1973	3.338	1976	2.992	1959	2.683
2146	3.405	2148	3.058	2127	2.748
2334	3.463	2344	3.124	2319	2.814
2557	3.521	2569	3.191	2551	2.889
2861	3.589	2852	3.267	2850	2.964

Table 7. O_2 Excess Adsorbed Amount on NaX Zeolite As a Function of Pressure at (288, 303, and 318) K

T/K = 288		T/K = 303		T/K = 318	
p	Q_{ads}	p	Q_{ads}	p	Q_{ads}
kPa	mmol·g^{-1}	kPa	mmol·g^{-1}	kPa	mmol·g^{-1}
15	0.025	14	0.014	17	0.016
40	0.069	40	0.049	42	0.042
66	0.111	67	0.084	77	0.078
91	0.154	94	0.120	101	0.103
117	0.195	120	0.153	153	0.152
150	0.248	151	0.192	177	0.176
181	0.297	178	0.223	214	0.213
210	0.343	214	0.268	240	0.239
244	0.395	248	0.311	278	0.274
278	0.447	280	0.348	317	0.311
316	0.505	321	0.398	348	0.339
354	0.561	366	0.451	394	0.382
400	0.629	411	0.504	435	0.419
468	0.724	468	0.569	494	0.473
570	0.862	580	0.688	596	0.560
678	1.003	690	0.802	715	0.659
787	1.140	808	0.921	825	0.749
901	1.276	917	1.028	935	0.836
1012	1.400	1035	1.136	1047	0.920
1126	1.522	1161	1.247	1173	1.010
1254	1.653	1281	1.348	1288	1.092
1378	1.771	1404	1.450	1416	1.178
1507	1.887	1535	1.547	1548	1.262
1641	2.000	1668	1.645	1687	1.349
1792	2.120	1815	1.744	1834	1.436
1952	2.236	1966	1.844	1983	1.518
2121	2.350	2138	1.947	2152	1.608
2306	2.465	2326	2.051	2350	1.703
2531	2.589	2551	2.165	2562	1.802
2840	2.741	2851	2.299	2848	1.920

Table 8. O_2 Excess Adsorbed Amount on NaLSX Zeolite As a Function of Pressure at (288, 303, and 318) K

T/K = 288		T/K = 303		T/K = 318	
p	Q_{ads}	p	Q_{ads}	p	Q_{ads}
kPa	mmol·g^{-1}	kPa	mmol·g^{-1}	kPa	mmol·g^{-1}
16	0.025	13	0.019	15	0.018
43	0.063	41	0.050	40	0.041
67	0.099	68	0.080	68	0.068
92	0.135	94	0.110	96	0.095
120	0.174	122	0.140	122	0.117
150	0.216	152	0.173	150	0.142
184	0.263	180	0.203	179	0.167
217	0.307	212	0.236	210	0.191
252	0.351	242	0.269	244	0.219
289	0.400	277	0.305	276	0.247
324	0.446	316	0.345	313	0.277
369	0.502	357	0.389	360	0.316
411	0.555	414	0.445	410	0.356
474	0.632	474	0.504	473	0.407
579	0.755	579	0.601	586	0.493
693	0.885	684	0.698	699	0.577
803	1.007	794	0.796	810	0.658
923	1.132	908	0.895	924	0.740
1035	1.245	1024	0.990	1041	0.819
1149	1.354	1141	1.083	1159	0.897
1272	1.464	1264	1.176	1279	0.973
1396	1.572	1391	1.269	1407	1.053
1530	1.680	1528	1.365	1539	1.131
1666	1.785	1661	1.453	1675	1.209
1811	1.890	1806	1.544	1822	1.289
1963	1.993	1962	1.636	1979	1.370
2133	2.096	2138	1.733	2146	1.452
2319	2.204	2332	1.834	2334	1.540
2546	2.323	2554	1.940	2560	1.636
2849	2.461	2847	2.066	2850	1.753

Table 9. O_2 Excess Adsorbed Amount on KLSX Zeolite As a Function of Pressure at (288, 303, and 318) K

T/K = 288		T/K = 303		T/K = 318	
p	Q_{ads}	p	Q_{ads}	p	Q_{ads}
kPa	mmol·g^{-1}	kPa	mmol·g^{-1}	kPa	mmol·g^{-1}
15	0.023	16	0.016	14	0.010
48	0.072	41	0.045	42	0.036
74	0.111	69	0.076	67	0.057
100	0.149	96	0.106	96	0.082
127	0.188	125	0.138	126	0.106
156	0.227	153	0.170	156	0.130
184	0.266	182	0.200	185	0.154
213	0.306	216	0.235	217	0.181
246	0.351	246	0.268	251	0.209
279	0.393	279	0.300	288	0.238
316	0.442	313	0.335	325	0.266
355	0.491	361	0.381	373	0.302
403	0.550	415	0.430	415	0.334
464	0.621	470	0.483	469	0.374
589	0.756	585	0.581	573	0.448
695	0.869	693	0.672	689	0.528
808	0.979	812	0.767	803	0.603
922	1.083	926	0.853	921	0.677
1039	1.185	1047	0.941	1042	0.746
1160	1.283	1159	1.017	1168	0.818
1284	1.380	1293	1.102	1286	0.883
1413	1.469	1429	1.185	1407	0.946
1545	1.557	1558	1.257	1539	1.011
1685	1.643	1694	1.331	1671	1.073
1828	1.725	1844	1.406	1820	1.137
1988	1.808	2003	1.477	1984	1.204
2158	1.889	2169	1.550	2155	1.271
2341	1.970	2345	1.619	2332	1.335
2554	2.053	2559	1.694	2555	1.407
2856	2.153	2852	1.786	2860	1.510

ature, the nitrogen was the most adsorbed compound. This could be due to the fact that those adsorbates, although having similar polarizabilities (N_2: $1.74 \cdot 10^{-3}$ nm^3, O_2: $1.60 \cdot 10^{-3}$ nm^3),[45] have different molecular quadrupole moments[46] (N_2 has a moment

Table 10. O_2 Excess Adsorbed Amount on LiLSX Zeolite As a Function of Pressure at (288, 303, and 318) K

T/K = 288		T/K = 303		T/K = 318	
p	Q_{ads}	p	Q_{ads}	p	Q_{ads}
kPa	mmol·g^{-1}	kPa	mmol·g^{-1}	kPa	mmol·g^{-1}
14	0.021	13	0.014	37	0.036
40	0.065	37	0.043	60	0.057
64	0.109	64	0.080	89	0.087
90	0.155	92	0.118	115	0.118
115	0.194	118	0.150	142	0.142
142	0.243	146	0.190	168	0.174
172	0.292	177	0.230	198	0.207
202	0.350	208	0.272	227	0.233
236	0.410	239	0.315	259	0.268
273	0.471	276	0.367	292	0.303
308	0.533	311	0.412	325	0.339
348	0.597	358	0.474	363	0.384
397	0.679	415	0.546	410	0.431
470	0.796	475	0.629	468	0.486
575	0.950	586	0.755	577	0.594
690	1.107	690	0.875	685	0.695
802	1.259	812	1.016	790	0.799
911	1.405	917	1.133	911	0.904
1027	1.545	1037	1.252	1024	1.003
1147	1.688	1156	1.374	1139	1.105
1270	1.834	1276	1.498	1262	1.208
1393	1.965	1406	1.625	1389	1.313
1521	2.097	1556	1.754	1529	1.420
1663	2.242	1685	1.867	1670	1.529
1810	2.370	1829	1.981	1808	1.631
1958	2.500	1985	2.108	1961	1.744
2124	2.633	2144	2.226	2134	1.849
2311	2.778	2329	2.357	2325	1.976
2541	2.924	2541	2.490	2537	2.095
2844	3.094	2853	2.655	2839	2.246

Table 11. O_2 Excess Adsorbed Amount on Homemade LiLSX^{hm} Zeolite As a Function of Pressure at (288, 303, and 318) K

T/K = 288		T/K = 303		T/K = 318	
p	Q_{ads}	p	Q_{ads}	p	Q_{ads}
kPa	mmol·g^{-1}	kPa	mmol·g^{-1}	kPa	mmol·g^{-1}
15	0.027	17	0.018	14	0.018
39	0.081	42	0.054	41	0.045
64	0.127	69	0.100	67	0.072
89	0.173	95	0.136	93	0.109
116	0.219	121	0.182	124	0.137
146	0.275	151	0.220	151	0.165
176	0.330	179	0.257	180	0.202
205	0.387	210	0.304	209	0.230
236	0.444	241	0.351	244	0.268
271	0.501	277	0.399	278	0.306
310	0.567	316	0.446	313	0.344
351	0.634	362	0.494	356	0.392
403	0.721	408	0.562	403	0.440
467	0.817	471	0.639	467	0.507
570	0.970	575	0.754	570	0.603
680	1.115	688	0.879	678	0.709
787	1.251	808	0.995	788	0.806
894	1.379	919	1.103	898	0.903
1012	1.517	1041	1.212	1011	1.002
1128	1.646	1164	1.321	1130	1.091
1254	1.766	1293	1.430	1252	1.190
1378	1.887	1425	1.531	1377	1.281
1503	2.000	1556	1.642	1508	1.362
1643	2.122	1695	1.744	1648	1.454
1793	2.236	1837	1.847	1808	1.536
1963	2.350	1984	1.950	1964	1.628
2128	2.465	2154	2.054	2126	1.712
2317	2.580	2349	2.168	2327	1.815
2538	2.696	2560	2.273	2541	1.909
2840	2.833	2847	2.408	2844	2.033

2.3 times higher than O_2) which are related to the interaction of the adsorbate with the compensation cation. To characterize

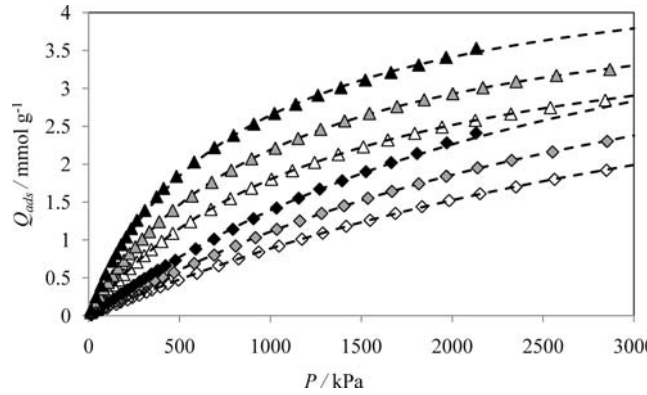

Figure 3. Excess adsorption isotherm on NaX: Δ, nitrogen; ◇, oxygen; black, 288 K; gray, 303 K; white, 318 K.

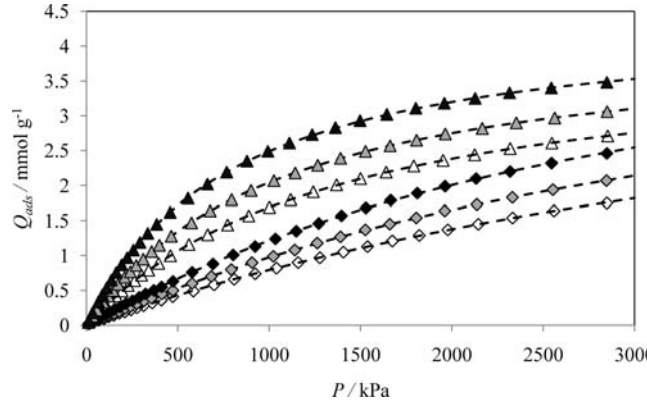

Figure 4. Excess adsorption isotherm on NaLSX: Δ, nitrogen; ◇, oxygen; black, 288 K; gray, 303 K; white, 318 K.

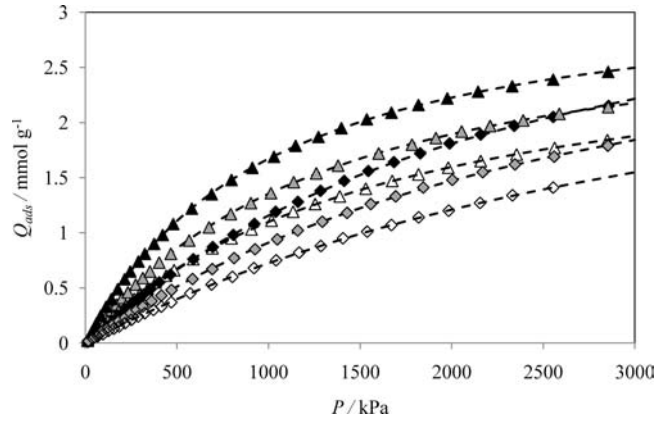

Figure 5. Excess adsorption isotherm on KLSX: Δ, nitrogen; ◇, oxygen; black, 288 K; gray, 303 K; white, 318 K.

the adsorbate−adsorbent interactions for the different cation exchanged X faujasite forms, we have determined the isosteric heat of adsorption at zero coverage (where the adsorbate−adsorbate interactions are negligible). Those values are evaluated from the Clausius−Clapeyron equation in the range of the experimental temperatures (288 K to 318 K) and are reported in Table 17. Those results will be discussed further in the paper.

In Table 18, we report the so-called working capacity,[47] defined as the difference between the amounts of nitrogen adsorbed at a typical total feed pressure (about 400 kPa for PSA) and at the evacuation pressure (100 kPa).

The experimental isotherms obtained for all the adsorbents and for each temperature have been used to calculate the

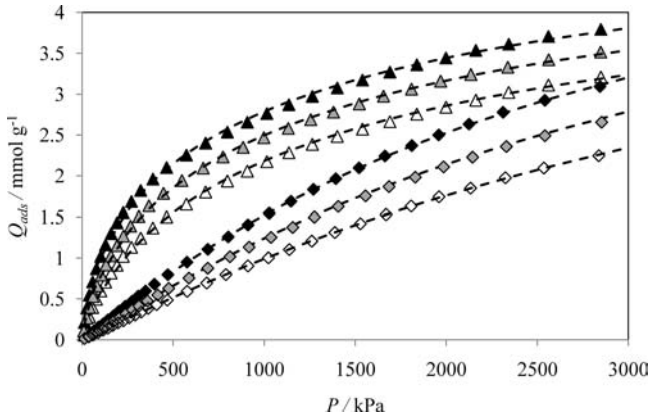

Figure 6. Excess adsorption isotherm on LiLSX: Δ, nitrogen; ◇, oxygen; black, 288 K; gray, 303 K; white, 318 K.

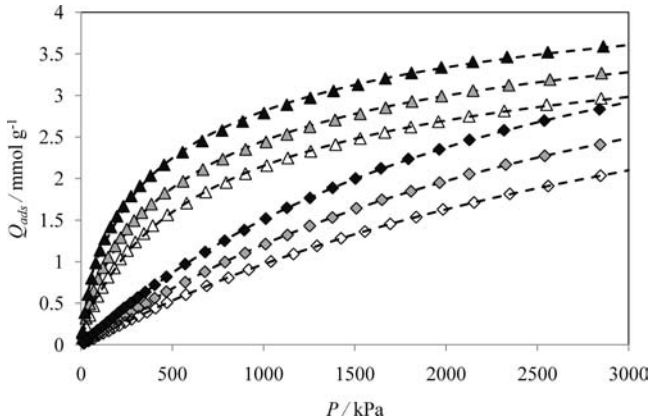

Figure 7. Excess adsorption isotherm on LiLSX^{hm}: Δ, nitrogen; ◇, oxygen; black, 288 K; gray, 303 K; white, 318 K.

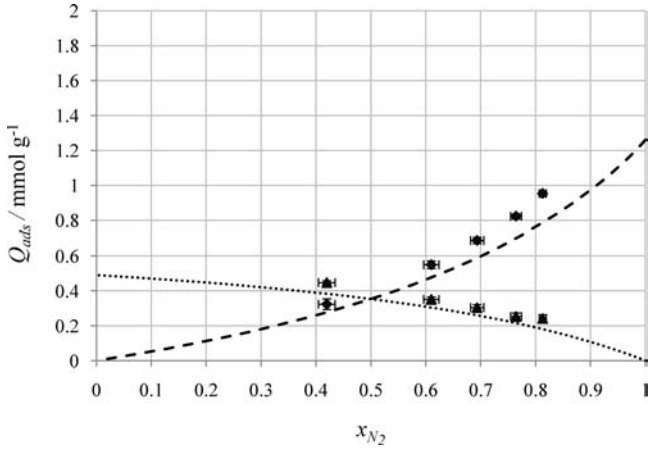

Figure 8. Coadsorption of N_2 and O_2 at 303 K and 400 kPa on NaX: ▲, oxygen; ◆, nitrogen; ---, Langmuir−Freundlich model.

Langmuir−Freundlich parameters by minimizing the following objective function

$$\text{O.F.} = (q_{\text{sim}} - q_{\text{exp}})^2 \quad (4)$$

where q_{sim} are the simulated adsorbed quantities and q_{exp} are the experimental adsorbed quantities.

Those parameters are reported in Table 19 and are used to simulate the coadsorption of nitrogen and oxygen (Figures 8 to 12).

Temperature Effect. In Figures 3 to 7, we can see the temperature influence on the adsorption capacities. For each gas and each adsorbent, the same behavior is observed: the adsorption capacity increases when the temperature decreases.

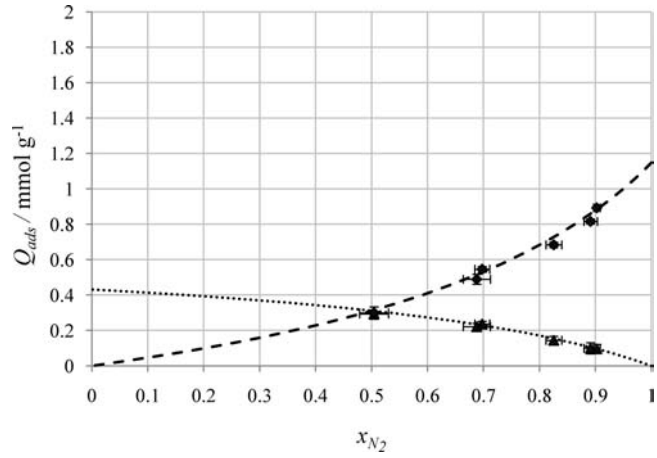

Figure 9. Coadsorption of N_2 and O_2 at 303 K and 400 kPa on NaLSX: ▲, oxygen; ◆, nitrogen; ---, Langmuir−Freundlich model.

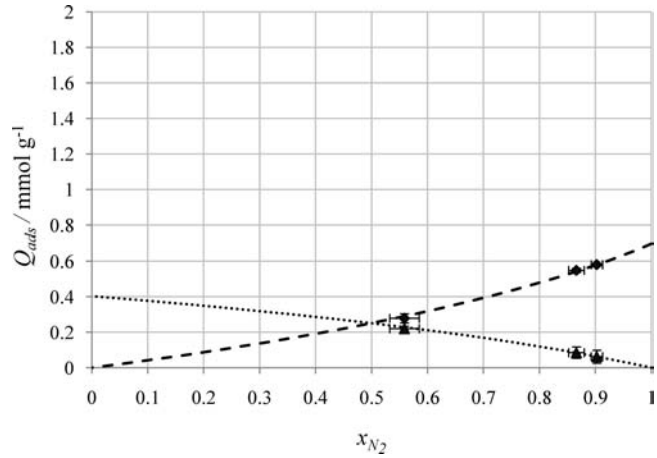

Figure 10. Coadsorption of N_2 and O_2 at 303 K and 400 kPa on KLSX: ▲, oxygen; ◆, nitrogen; ---, Langmuir−Freundlich model.

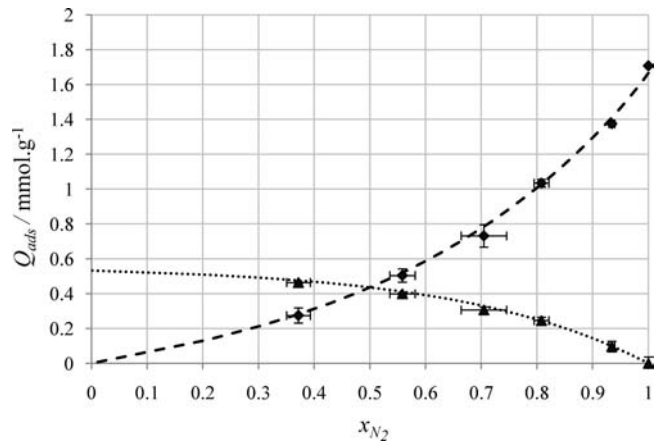

Figure 11. Coadsorption of N_2 and O_2 at 303 K and 400 kPa on LiLSX: ▲, oxygen; ◆, nitrogen; ---, Langmuir−Freundlich model.

Si/Al Ratio Influence. By comparing adsorption capacities for nitrogen and oxygen onto zeolites NaX and NaLSX (Figures 3 and 4), it is clear that NaX has a higher adsorption capacity. Similarly, the NaX working capacity is clearly higher than the NaLSX one. However, in the case of the coadsorption isotherms (Figures 8 and 9) for the same nitrogen fraction in the gas phase (y_{N_2}), the fraction of nitrogen adsorbed (x_{N_2}) is larger on NaLSX than on NaX, so the selectivity of the NaLSX zeolite is better.

Compensation Cation Effects. With the four zeolites with the same Si/Al ratio but with different cations (NaLSX, KLSX,

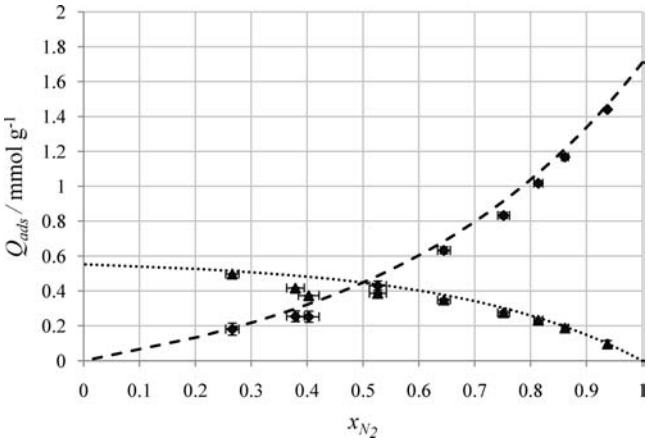

Figure 12. Coadsorption of N_2 and O_2 at 303 K and 400 kPa on LiLSX^{hm}: ▲, oxygen; ◆, nitrogen; ---, Langmuir−Freundlich model.

Table 12. Experimental Equilibrium Data for Oxygen and Nitrogen Coadsorption at 303 K and 400 kPa on NaX Zeolite

q_{N_2} / mmol·g^{-1}	q_{O_2} / mmol·g^{-1}	y_{N_2}	x_{N_2}
0.95 ± 0.02	0.24 ± 0.01	0.650 ± 0.001	0.813 ± 0.006
0.82 ± 0.02	0.25 ± 0.01	0.551 ± 0.001	0.76 ± 0.01
0.69 ± 0.02	0.30 ± 0.01	0.454 ± 0.001	0.69 ± 0.01
0.55 ± 0.01	0.35 ± 0.01	0.362 ± 0.001	0.61 ± 0.01
0.32 ± 0.01	0.45 ± 0.01	0.228 ± 0.001	0.42 ± 0.01

Table 13. Experimental Equilibrium Data for Oxygen and Nitrogen Coadsorption at 303 K and 400 kPa on NaLSX Zeolite

q_{N_2} / mmol·g^{-1}	q_{O_2} / mmol·g^{-1}	y_{N_2}	x_{N_2}
0.89 ± 0.01	0.10 ± 0.02	0.779 ± 0.001	0.903 ± 0.006
0.82 ± 0.01	0.10 ± 0.03	0.685 ± 0.001	0.89 ± 0.01
0.68 ± 0.01	0.14 ± 0.02	0.579 ± 0.001	0.83 ± 0.01
0.55 ± 0.01	0.24 ± 0.01	0.484 ± 0.001	0.70 ± 0.01
0.49 ± 0.02	0.22 ± 0.02	0.386 ± 0.001	0.69 ± 0.02
0.30 ± 0.02	0.29 ± 0.01	0.271 ± 0.001	0.50 ± 0.02

Table 14. Experimental Equilibrium Data for Oxygen and Nitrogen Coadsorption at 303 K and 400 kPa on KLSX Zeolite

q_{N_2} / mmol·g^{-1}	q_{O_2} / mmol·g^{-1}	y_{N_2}	x_{N_2}
0.58 ± 0.01	0.06 ± 0.01	0.818 ± 0.002	0.90 ± 0.01
0.55 ± 0.01	0.09 ± 0.01	0.734 ± 0.003	0.87 ± 0.01
0.27 ± 0.02	0.22 ± 0.02	0.337 ± 0.002	0.56 ± 0.02

Table 15. Experimental Equilibrium Data for Oxygen and Nitrogen Coadsorption at 303 K and 400 kPa on LiLSX Zeolite

q_{N_2} / mmol·g^{-1}	q_{O_2} / mmol·g^{-1}	y_{N_2}	x_{N_2}
1.71 ± 0.03	0	1	1
1.38 ± 0.03	0.096 ± 0.008	0.759 ± 0.001	0.934 ± 0.005
1.03 ± 0.02	0.25 ± 0.02	0.433 ± 0.001	0.81 ± 0.01
0.73 ± 0.02	0.31 ± 0.05	0.201 ± 0.001	0.70 ± 0.04
0.503 ± 0.008	0.40 ± 0.04	0.148 ± 0.001	0.56 ± 0.02
0.274 ± 0.004	0.46 ± 0.05	0.064 ± 0.001	0.37 ± 0.02

LiLSX, and LiLSX^{hm}) (Figures 4 to 7), it appears that the maximum adsorbed quantity is obtained for LiLSX, probably due to the fact that this adsorbent is characterized by a higher specific surface area (Table 1). The lowest adsorbed quantity is obtained for KLSX. For comparing the adsorption capacities, it is interesting to express some results in terms of molecules per supercage to eliminate the effect of molecular weight in the different exchanged zeolites. Indeed, K is heavier than Li, so for the same mass of zeolite, the one with the smallest cation

Table 16. Experimental Equilibrium Data for Oxygen and Nitrogen Coadsorption at 303 K and 400 kPa on LiLSX^{hm} Zeolite

q_{N_2} / mmol·g^{-1}	q_{O_2} / mmol·g^{-1}	y_{N_2}	x_{N_2}
1.44 ± 0.01	0.096 ± 0.004	0.713 ± 0.001	0.938 ± 0.003
1.17 ± 0.01	0.19 ± 0.01	0.470 ± 0.001	0.862 ± 0.006
1.02 ± 0.01	0.23 ± 0.02	0.376 ± 0.001	0.81 ± 0.01
0.832 ± 0.008	0.27 ± 0.01	0.258 ± 0.001	0.75 ± 0.01
0.632 ± 0.006	0.35 ± 0.02	0.204 ± 0.001	0.64 ± 0.02
0.430 ± 0.004	0.39 ± 0.02	0.100 ± 0.001	0.53 ± 0.02
0.254 ± 0.002	0.42 ± 0.03	0.038 ± 0.001	0.38 ± 0.03
0.180 ± 0.001	0.50 ± 0.03	0.017 ± 0.001	0.26 ± 0.03

Table 17. Ionic Radii[50] of the Cation, Isosteric Heats of Adsorption at Zero Coverage, and 288 K Isotherm Slopes in the Henry's Region for Both Nitrogen and Oxygen

		nitrogen		oxygen	
	cation radius	ΔH_{ads}	slope	ΔH_{ads}	slope
adsorbent	Å	kJ·mol^{-1}	mmol·g^{-1}·kPa^{-1}	kJ·mol^{-1}	mmol·g^{-1}·kPa^{-1}
LiLSX	0.68	25.85	0.0160	13.44	0.0017
LiLSX^{hm}	0.68	27.80	0.0188	13.02	0.0019
NaX	0.97	17.97	0.0062	13.46	0.0017
NaLSX	0.97	17.20	0.0051	10.37	0.0015
KLSX	1.33	16.03	0.0030	13.04	0.0015

Table 18. Working Capacities

zeolite	working capacity
NaX	0.85
NaLSX	0.79
KLSX	0.51
LiLSX	0.94
LiLSX^{hm}	0.90

(Li in this study) contains more supercages than the others. To realize this unit conversion, we have used the chemical formula for the unit cells provided in Table 1 knowing that X-faujasites contain eight supercages per unit cell. The chosen pressures are (320 and 80) kPa for, respectively, nitrogen and oxygen. Those values correspond to the partial pressure of each component for a total air feed pressure of 400 kPa which is a typical feed pressure for a PSA process. The results are reported in Table 20.

For nitrogen, we can observe that adsorbed quantities expressed in molecules per supercage increase in the sequence Li > Na > K.

This behavior has already been pointed out by McKee.[48] With adsorbents having the same Si/Al ratio = 1, the adsorption capacity increases in inverse proportion to the size of the compensation cation:[29] the capacity is higher for lithium which has the smallest atomic radius (0.68 Å) and smaller for the potassium which has the largest atomic radius (1.33 Å). This effect can be explained by the fact that for a smaller compensation cation the specific surface area of the adsorbent is larger (Table 1). However, for oxygen, those capacities seem to be more or less constant which could say that the extra-framework cation has less influence for oxygen adsorption than for the nitrogen one.

In this case of different cation exchanged zeolites, it is also interesting to compare the energetic behavior. Indeed, according to the considered cation, the adsorbate−adsorbent interactions are different. To characterize those interactions, we compare the isosteric heats of adsorption at zero coverage (adsorbate−adsorbate interactions are negligible) and the isotherm slopes at 288 K at the low-pressure region corresponding to the Henry's region for both nitrogen and oxygen. Those slopes are directly related to the adsorbate−adsorbent interactions. All values are reported in Table 17 for the five zeolite forms. However, the

Table 19. Langmuir−Freundlich Parameters

		nitrogen			oxygen		
	temperature	q_S	b		q_S	b	
adsorbent	K	mmol·g^{-1}	kPa$^{-\alpha}$	α	mmol·g^{-1}	kPa$^{-\alpha}$	α
NaX	288	4.977	$1.675 \cdot 10^{-3}$	0.944	6.132	$2.914 \cdot 10^{-4}$	1.000
	303	4.510	$1.163 \cdot 10^{-3}$	0.970	5.794	$2.353 \cdot 10^{-4}$	1.000
	318	4.244	$8.263 \cdot 10^{-4}$	0.983	5.419	$1.951 \cdot 10^{-4}$	1.000
NaLSX	288	4.487	$1.241 \cdot 10^{-3}$	1.000	5.853	$2.603 \cdot 10^{-4}$	1.000
	303	4.219	$9.357 \cdot 10^{-4}$	1.000	5.465	$2.163 \cdot 10^{-4}$	1.000
	318	4.054	$7.132 \cdot 10^{-4}$	1.000	5.158	$1.826 \cdot 10^{-4}$	0.999
KLSX	288	3.359	$9.823 \cdot 10^{-4}$	1.000	4.199	$3.775 \cdot 10^{-4}$	1.000
	303	3.173	$7.395 \cdot 10^{-4}$	1.000	3.878	$3.053 \cdot 10^{-4}$	1.000
	318	2.933	$5.977 \cdot 10^{-4}$	1.000	3.707	$2.417 \cdot 10^{-4}$	1.000
LiLSX	288	5.915	$1.036 \cdot 10^{-2}$	0.645	7.436	$2.562 \cdot 10^{-4}$	1.000
	303	5.479	$6.232 \cdot 10^{-3}$	0.709	7.342	$2.006 \cdot 10^{-4}$	1.000
	318	5.062	$3.569 \cdot 10^{-3}$	0.776	7.195	$1.605 \cdot 10^{-4}$	1.000
LiLSX^{hm}	288	4.843	$1.269 \cdot 10^{-2}$	0.679	5.604	$3.669 \cdot 10^{-4}$	1.000
	303	4.530	$7.790 \cdot 10^{-3}$	0.727	5.417	$2.808 \cdot 10^{-4}$	1.000
	318	4.153	$4.752 \cdot 10^{-3}$	0.785	4.979	$2.466 \cdot 10^{-4}$	1.000

Table 20. Nitrogen and Oxygen Adsorption Capacities at, Respectively, (320 and 80) kPa

	nitrogen		oxygen	
	Q_{ads}	Q_{ads}	Q_{ads}	Q_{ads}
adsorbent	mmol·g^{-1}	molec·sc^{-1}	mmol·g^{-1}	molec·sc^{-1}
LiLSX	1.67	2.53	0.55	0.83
LiLSX^{hm}	1.71	2.59	0.55	0.83
NaLSX	1.15	1.96	0.44	0.74
KLSX	0.72	1.37	0.42	0.80

following discussion is based on only the three commercial LSX forms (LiLSX, NaLSX, and KLSX) which are provided by the same company.

For nitrogen, we can observe that the isosteric heats of adsorption at zero coverage and the isotherm slopes at 288 K increase in the sequence Li > Na > K, when the ionic radius of the extra-framework cations decreases. Those trends have already been observed in previous studies for different adsorbates like nitrogen,[29,49] argon,[29] carbon monoxide,[49] or carbon dioxide.[50] Furthermore, the ΔH_{ads} at zero coverage of 25 kJ·mol^{-1} on LiLSX is in the same order of magnitude as the one observed by Yoshida et al.[28] Different types of contributions can play a role in the interaction between adsorbate and the extra-framework cation like polarization effect, electrostatic contribution, or acid−base effect for acidic adsorbate (e.g., CO_2). In the case of nitrogen, Maurin et al.[29] have shown that polarization and electrostatic contributions (nitrogen is characterized by a permanent quadrupole moment) occur. As those effects are both conversely proportional to the distance, the smaller the cations, the larger the interactions. So, the adsorbate−adsorbent interactions increase with the charge density. Moreover, a linear relationship is observed between the isosteric heat of adsorption at zero coverage and the isotherm slopes at 288 K as we can see in Figure 13. It seems logical given that those two values characterize the first adsorbate−adsorbent interactions.

For oxygen, the relationship between isosteric heat of adsorption at zero coverage and isotherm slope does not present the same behavior. It can be due to the weak values of the isotherm slopes which are comprised in the experimental incertitude. However, those values seem to be more or less constant, and the values of the isosteric heat of adsorption at zero coverage are all in the same order of magnitude (13 kJ·mol^{-1}) except for the NaLSX for which the isosteric heat of adsorption is abnormally weak. It could be said that for oxygen the effect of the extra-framework cation is less important than for nitrogen and could be explicated by the difference of the quadrupole moments. Savitz et al.[49] have shown that the extra-framework cation does not affect the oxygen adsorption on MFI, the isosteric heat of adsorption being the same for Li- or K-exchanged MFI. Moreover, a value of 13 kJ·mol^{-1} for ΔH_{ads} at zero coverage is confirmed by the study of Shen et al.[51] To conclude this energetic discussion, we can see that homemade LiLSX presents larger adsorbate−adsorbent interaction at zero coverage than LiLSX. However, as presented below, the capacities are greater for LiLSX probably due to a larger Li exchange rate. The difference between the two exchange rates seems to be too small to influence the energetic behavior.

Concerning the working capacity, the same conclusions can be made, with lower values for KLSX and higher values for LiLSX. LiLSX^{hm}, which contains less Li cations than LiLSX, has also a lower working capacity. The amount of Li exchanged cations appears to have a major effect on the working capacity.

We can see in Figures 9 to 12, that for the same nitrogen molar fraction y_{N2} (close to 0.79 for air composition) the ratio of nitrogen adsorbed is smaller for the NaLSX and KLSX zeolites than for LiLSX and LiLSX^{hm}. For use in oxygen purification from air, LiLSX provided by Tricat and homemade LiLSX zeolites would be the more efficient zeolites because they present larger adsorption capacities and better selectivities. We can note that, although the two LiLSX zeolites have the same selectivity, the adsorption capacity of LiLSX provided by Tricat is larger, certainly due to its larger specific surface area and the higher amount of the Li cation. Actually, with over 70 % of Li exchanged, sites SI′ and SII are fully occupied by

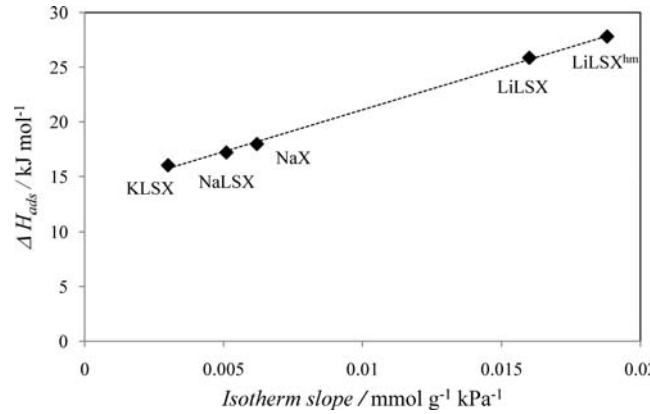

Figure 13. Linear relationship between the isosteric heat of adsorption at zero coverage (ΔH_{ads}) and the nitrogen isotherm slope at 288 K.

the lithium cation, and the population of site SIII occupied by Li increases. The nitrogen adsorption capacity increases also with site SIII occupation.[23,30] The homemade LiLSX is exchanged at a rate of 98.2 %, while it reaches 98.4 % for the one provided by Tricat.

Coadsorption Equilibrium Prediction. In Figures 8 to 12, the results of the extended Langmuir−Freundlich model are reported. Adsorbed quantities are well-predicted with an average deviation lower than 0.4 % for NaX and lower than 0.1 % for other zeolites. This model allows a good prediction of adsorbed quantities for binary nitrogen/oxygen mixtures.

Conclusions

In this paper, we present excess adsorption isotherms for pure nitrogen and oxygen on five zeolites (NaX, NaLSX, KLSX, LiLSX, homemade $LiLSX^{hm}$) for pressures ranging from (0 to 3 000) kPa and for temperatures ranging from (288 to 318) K and a coadsorption isotherm at 400 kPa and 303 K.

With Na as the compensation cation, the best results are obtained for a Si/Al ratio equal to 1 if used for oxygen purification in a PSA process but with a weaker working capacity and a better selectivity. With this Si/Al ratio value, it is clear that Li compensation cation exchange can improve adsorption capacities and selectivity of the adsorbent. In the set of the zeolites used in this study, LiLSX appears to be the best zeolite for a PSA process for oxygen purification. Nevertheless, the homemade LiLSX has given promising results, and we hope to enhance these capacities by improving the amount of the Li cation substituted.

Literature Cited

(1) Talu, O.; Li, J.; Kumar, R.; Mathias, P. M.; Moyer, J. D.; Schork, J. M. Measurements and analysis of oxygen/nitrogen/5A-zeolite adsorption equilibria for air separartion. *Gas. Sep. Purif.* **1996**, *10*, 149–159.

(2) Crittenden, B. D.; Thomas, W. J. *Adsorption Technology and Design*; Butterworth - Heinemann: Oxford, 1998.

(3) Finlayson, D.; Sharp, A. J. Separating gaseous mixtures. *UK Patent 365,092 19301015*, 1930.

(4) Skarstrom, C. W. Fractionating gas mixtures by adsorption. *US Patent 2,944,627 19600712*, 1960.

(5) Rege, S. U.; Yang, R. T.; Buzanowski, M. A. Sorbents for air prepurification in air separation. *Chem. Eng. Sci.* **2000**, *55*, 4827–4838.

(6) Castle, W. F. Air separation and liquefaction: recent developments and prospects for the beginning of the new millennium. *Int. J. Refrigeration* **2002**, *25*, 158–172.

(7) Huang, M.-R.; Li, X.-G. Preparation and air-separation properties of membrane blends of low-molecular-weight liquid crystals with cellulose derivatives. *Gas. Sep. Purif.* **1995**, *9*, 87–92.

(8) Ruaan, R.-C.; Chen, S.-H.; Lai, J.-Y. Oxygen/nitrogen separation by polycarbonate/Co(SalPr) complex membranes. *J. Membr. Sci.* **1997**, *135*, 9–18.

(9) Ismail, A. F.; David, L. I. B. A review on the latest development of carbon membranes for gas separation. *J. Membr. Sci.* **2001**, *193*, 1–18.

(10) Reiβ, G. Status and development of oxygen generation processes on molecular sieve zeolites. *Gas. Sep. Purif.* **1994**, *8*, 95.

(11) Kumar, R. Vacuum swing adsorption process for oxygen production a historical perspective. *Sep. Sci. Technol.* **1996**, *31*, 877.

(12) Chahbani, M. H.; Tondeur, D. Mass transfer kinetics in pressure swing adsorption. *Sep. Purif. Technol.* **2000**, *20*, 185–196.

(13) Huang, W.-C.; Chou, C.-T. A moving finite element simulation of a pressure swing adsorption process. *Comput. Chem. Eng.* **1997**, *21*, 301–315.

(14) Shuai, X.; Cheng, S.; Meisen, A. Simulation of pressure swing adsorption modules having laminated structure. *Microporous Mater.* **1996**, *5*, 347–355.

(15) Serbezov, A.; Sotirchos, S. V. Particle-bed model for multicomponent adsorption-based separations: application to pressure swing adsorption. *Chem. Eng. Sci.* **1999**, *54*, 5647–5666.

(16) Budner, Z.; Dula, J.; Podstawa, W.; Gawzik, A. Study and modelling of the vacuum swing adsorption (VSA) process employed in the production of oxygen. *Trans IChemE.* **1999**, *77*, 405–412.

(17) Todd, R. S.; Webley, P. A. Macropore diffusion dusty-gas coefficient for pelletised zeolites from breakthrough experiments in the O_2/N_2 system. *Chem. Eng. Sci.* **2005**, *60*, 4593–4608.

(18) Mendes, A. M. M.; Costa, C. A. V.; Rodrigues, A. E. Oxygen separation from air by PSA: modelling and experimental results. Part I: isothermal operation. *Sep. Purif. Technol.* **2001**, *24*, 173–188.

(19) Rege, S. U.; Yang, R. T. Limits for air separation by adsorption with LiX zeolite. *Ind. Eng. Chem. Res.* **1997**, *36*, 5358–5365.

(20) Izumi, J.; Suzuki, M. Oxygen selectivity on partially K exchanged Na-A type zeolite at low temperature. *Adsorption* **2001**, *7*, 27–39.

(21) Izumi, J.; Suzuki, M. Oxygen selectivity on Na-A type zeolite at low temperature. *Adsorption* **2000**, *6*, 205–212.

(22) Izumi, J.; Suzuki, M. Oxygen selectivity of calcined Na-A type zeolite. *Adsorption* **2000**, *6*, 23–31.

(23) Yoshida, S.; Ogawa, N.; Kamioka, K.; Hirano, S.; Mori, T. Study of zeolite molecular sieves for production of oxygen by using pressure swing adsorption. *Adsorption* **1999**, *5*, 57–61.

(24) Talu, O.; Li, J.; Kumar, R.; Mathias, P. M.; Moyer, J. D.; Schork, J. M. Measurement and analysis of oxygen/nitrogen/5A-zeolite adsorption equilibria for air separation. *Gas. Sep. Purif.* **1996**, *10*, 149–159.

(25) Rege, S. U.; Yang, R. T.; Qian, K.; Buzanowski, M. A. Air-prepurification by pressure swing adsorption using single/layered beds. *Chem. Eng. Sci.* **2001**, *56*, 2745–2759.

(26) Park, J.-H.; Kim, J.-N.; Cho, S.-H.; Kim, J.-D.; Yang, R. T. Adsorber dynamics and optimal design of layered beds for multicomponent gas adsorption. *Chem. Eng. Sci.* **1998**, *53*, 3951–3963.

(27) Arvind, R.; Farooq, S.; Ruthven, D. M. Analysis of a piston PSA process for air separation. *Chem. Eng. Sci.* **2002**, *57*, 419–433.

(28) Yoshida, S.; Hirano, S.; Harada, A. Nitrogen adsorption properties of cubic and orthorhombic Li-exchanged low silica X. *Microporous Mesoporous Mater.* **2001**, *40*, 203–209.

(29) Maurin, G.; Llewellyn, P. L.; Poyet, T.; Kuchta, B. Adsorption of argon and nitrogen in X-faujasites: relationships for understanding the interactions with monovalent and divalent cations. *Microporous Mesoporous Mater.* **2005**, *79*, 53–59.

(30) Feuerstein, M.; Engelhardt, G.; McDaniel, P. L.; MacDougall, J. E.; Gaffney, T. R. Solid-state nuclear magnetic resonance investigation of cation siting in LiNaLSX zeolites. *Microporous Mesoporous Mater.* **1998**, *26*, 27–35.

(31) Li, Y. Y.; Perera, S. P.; Crittenden, B. D. Zeolite monoliths for air separation Part 1: Manufacture and Characterization. *Trans IChemE* **1998**, *76*, 921–930.

(32) Belmabkhout, Y.; Frère, M.; De Weireld, G. High-pressure adsorption measurements. A comparative study of the volumetric and gravimetric methods. *Meas. Sci. Technol.* **2004**, *15*, 1–11.

(33) Olivier, M.-G.; Lienard, O.; Jadot, R. Isobaric measurement of the adsorption selectivity curves of binary gaseous mixtures on microporous media. *Meas. Sci. Technol.* **1996**, *7*, 185–191.

(34) Jee, J.; Lee, S. Three-bed PVSA process for high-purity O_2 generation from ambient air. *AIChE J.* **2005**, *41*, 2988–2999.

(35) Murata, K.; Miyawaki, J.; Kaneko, K. A simple determination method of the absolute adsorbed amount for high pressure gas adsorption. *Carbon* **2002**, *40*, 425–428.

(36) De Weireld, G.; Frère, M.; Jadot, R. Characterization of porous carbonaceous sorbents using high pressure-high temperature adsorption data. *Stud. Surf. Sci. Catal.* **2000**, *128*, 333–345.

(37) Kunz, O.; Klimeck, R.; Wagner, W.; Jaeschke, M. The GERG-2004 Wide-Range Reference Equation of State for Natural Gases and Other Mixtures. *GERG Technical Monograph. Fortschr.-Ber.* VDI; VDI-Verlag: Düsseldorf, 2006.

(38) Yang, J.; Hana, S.; Chob, C.; Lee, C.-H.; Lee, H. Bulk separation of hydrogen mixtures by a one-column PSA. *Sep. Technol.* **1995**, *5*, 239–249.

(39) Kim, W.-G.; Yang, J.; Hana, S.; Chob, C.; Lee, C.-H.; Lee, H. Experimental and theoretical study on H_2/CO_2 separation by a five-step one-column PSA process. *Korean J. Chem. Eng.* **1995**, *12*, 503–511.

(40) Span, R.; Lemmon, E. W.; Jacobsen, R. T.; Wagner, W.; Yokozeki, A. A Reference Quality Thermodynamic Property Formulation for Nitrogen. *J. Phys. Chem. Ref. Data* **2000**, *29*, 1361–1433.

(41) Tegeler, C.; Span, R.; Wagner, W. A New Equation of State for Argon Covering the Fluid Region for Temperatures from the Melting Line to 700 K at Pressures up to 1000 MPa. *J. Phys. Chem. Ref. Data* **1999**, *28*, 779–850.

(42) Berlier, K.; Bougard, J.; Olivier, M. G. Automated measurement of isotherms of adsorption on microporous media in large ranges of pressure and temperature. *Meas. Sci. Technol.* **1995**, *6*, 107–113.

(43) De Weireld, G.; Frère, M. Study of the buoyancy effect on high pressure and high temperature adsorption isotherms measurements. *Proceedings of FOA7*; IK International, Ltd.: Chiba City, 2001; pp 693−699.

(44) Rege, S. U.; Yang, R. T.; Buzanow, M. A. Sorbents for air prepurification in air separation. *Chem. Eng. Sci.* **2000**, *55*, 4827–4838.
(45) Ross, S.; Olivier, J. P. *On physical adsorption*; Interscience: New York, 1964.
(46) Kazansky, V. B.; Bülow, M.; Tichomirova, E. Specific sorption sites for nitrogen in zeolites NaLSX and LiLSX. *Adsorption* **2001**, *7*, 291–299.
(47) Gaffney, T. H. Porous solid for air separation. *Curr. Opin. Solid. State Mater. Sci.* **1996**, *1*, 69–75.
(48) McKee, D. W. Separation of an oxygen-nitrogen mixture. *US Patent 3,140,933 19640714*, 1964.
(49) Savitz, S.; Myers, A. L.; Gorte, R. J. A calorimetric investigation of CO, N_2, and O_2 in alkali-exchanged MFI. *Microporous Mesoporous Mater.* **2000**, *37*, 33–40.
(50) Walton, K. S.; Abney, M. B.; LeVan, M. D. CO_2 adsorption in Y and X zeolites modified by alkali metal cation exchange. *Microporous Mesoporous Mater.* **2006**, *91*, 78–84.
(51) Shen, D.; Bülow, M.; Jale, S. R.; Fitch, F. R.; Ojo, A. F. Thermodynamics of nitrogen and oxygen sorption on zeolites LiLSX and CaA. *Microporous Mesoporous Mater.* **2001**, *48*, 211–217.

Received for review June 26, 2009. Accepted November 6, 2009. This work was supported by the Department for Technology, Research and Energy of the Walloon Region DGTRE (Belgium).

JE900539M